Computer Assisted Mechanics and Engineering Sciences, 5: 399–420, 1998.

New predictor-corrector method used as a solver for decohesion problem

Maciej Kowalczyk
Institute of Fundamental Technological Research PAS
Świętokrzyska 21, Warsaw 00-049, Poland

(Received December 22, 1997)

In certain problems of loading of elastic-perfectly plastic thin sheets a continuous displacement solution may not exist. The evolution of plastic zone is then connected with the evolution of discontinuity lines in both velocity and displacement fields. In the present paper it is assumed that in the presence of discontinuity lines the localized plastic zones start to proceed. A numerical study of decohesion within thin elastic-plastic sheets is conducted to total collapse. It is shown, that the localized plastic flow may develop simultaneously with the diffuse plastic zones. The structural softening caused by decohesive cracks is coupled with a complex elasto-plastic deformation process, where the previously developed diffuse plastic zones are subjected to unloading. The post-critical analysis is performed using a new reliable algorithm of a continuation method. The algorithm is based on a rank analysis of the rectangular matrix of the homogeneous set of incremental equations.

1. Introduction

In real structures the changes in geometry often arise from the formation of new free surfaces resulting from the decohesion processes. The initiation of material failure may take various forms, either as a result of void nucleation, growth and coalescence, or crack initiation and growth. Several sophisticated material models have been proposed in the literature in order to capture such processes. For example, the effects of void nucleation and growth within large deformation theory with account for hardening and softening effects were treated by Needleman [1] and Tvergaard [2]. The problem with decohesion can also occur, when the material is treated much simpler as an elastic-perfectly plastic either within the framework of small strain (see, Życzkowski and Tran-le Binh [3]) or finite strain theories (see, Życzkowski and Szuwalski [4]). When the structural material is treated as an elastic-perfectly plastic, a continuous displacement solution may not exist and the evolution of plastic zone is connected with the evolution of inadmissible discontinuity lines in both velocity and displacement fields. The formation of discontinuity lines may be regarded as an upper bound to all criteria of decohesion ([3]). Under force-controlled loadings the decohesion proceeds as a brittle rupture, however, for other boundary control such as prescribed displacements, a structure can be loaded well beyond the loading limit point.

The material instability may be regarded as the loss of ellipticity, when the positive definiteness of acoustic tensor is lost. As the failure is intimately connected to material behavior, one may construct the unified constitutive equations, which yield the correct discontinuous mode in addition to stress-strain responses prior to post-critical responses ([1, 2]). However, a quite different approach can be encountered, when the governing set of equations is augmented by a separate function relating the traction components and displacement discontinuities along the localization zone. The simplified exponential relation between the driving decohesion force and the displacement jump at the interface was presented in the theoretical paper by Schreyer and Zhou [5]. In the case of elastic-perfectly plastic material model Hill [6] proposed a treatment of discontinuity lines as the onset of a continuous necking process. Obviously, necking results with the ultimate crack formation

and softening behavior. Such physical idea was utilized by Mróz and Kowalczyk [7] for the problems of thin sheets with the localization mode constituted by out-of-plane shearing. In general, the aim of additional relations is to describe the failure modes and preserve the problem well posed. The complete analysis in a real structure within finite strain theories and sophisticated material models might be extremely expensive. Much cheaper calculations within small strain theory seem to be more attractive, as the large strains are confined within the plastic decohesion zone.

The decohesion within any part of the structure induces a nonlinear character of the deformation process. The nonlinear analysis can be conveniently performed using finite element modeling and continuation (or path-following) methods, which are well described in many textbooks (see, for example, [13, 14, 15]). Within continuation algorithms the incremental set of equations is augmented by the so-called constraint equation. It is obvious since the beginning of investigations on path-following algorithms (see [16]) that the Jacobian of augmented incremental system should be nonsingular. The experience indicates that this fundamental condition can not be fulfilled, when the procedures are tested on a great variety of problems. For example, the limit capacity of elastic-perfectly plastic structures defines the mathematical limit for usefulness of the well known continuation schemes. When the ultimate loading becomes constant and strains and displacements increase into infinity (see, [17]), the problem with singularity of tangent stiffness matrix can not be removed by any kind of augmentation. The physical validity of the limit state theory is obviously confined, but the loss of its significance does not necessary occur immediately, when the loading approaches its maximum. When perfectly plastic material is analyzed together with softening caused by decohesion, the problem with ill-conditioned tangent stiffness matrices becomes extremely severe.

In the present paper, the evolution of decohesive cracks within the elastic-perfectly plastic thin sheets is studied numerically. The simultaneous development of diffusive plasticity and decohesive cracks propagation is analyzed until the complete separation at the interface. The material behavior in a localized zone is described in terms of the formula proposed in [7] and the cracks are modeled by the interface elements. The elastic-perfectly plastic material model together with the Huber-Mises yield condition and the associated flow rule are used within the diffusive plastic zone. The calculations are effectively performed by the new compatible procedure proposed by Kowalczyk [18, 19]. The method is based on rank analysis of the matrix of the incremental set of equations written in a homogeneous form. The rank analysis is used in order to generate automatically the control variables at each step during the iteration process. The constraint equation is not defined in an explicit form. It is shown, that the control variables induced by the algorithm have their important physical meaning within the considered problem.

2. Preliminary example

As an introductory example into the problems of elasto-plastic deformation in the presence of discontinuity lines consider the annular disk uniformly loaded by the pressure p at its external boundary $r = b$ and rigidly supported at the interior boundary $r = a$ (see Fig. 1). The thin disks are analyzed with the thickness H small in comparison to a, i.e. $H \ll a$, so the plane stress assumption is justified. The discussion is confined to the prerequisites for an assumption, that the appearance of the displacement discontinuity lines can be interpreted as an onset of the localized flow. Since the large deformation process is confined to a narrow cohesive zone, the analysis of the whole structure is conducted within the small strain theory. The complete solution of the problem was presented by Mróz and Kowalczyk in [7].

Denote by $u(r,t)$ the radial displacement, by $\varepsilon_r, \varepsilon_t$ the radial and circumferential strain components and by σ_r, σ_t the respective stress components. The elastic deformation of the disk is described by a solution of the set of equations composed of the equilibrium condition, the Hooke's law and the geometric relation between the strain components and radial displacement. Neglecting the thickness variation, the respective relations are specified as follows

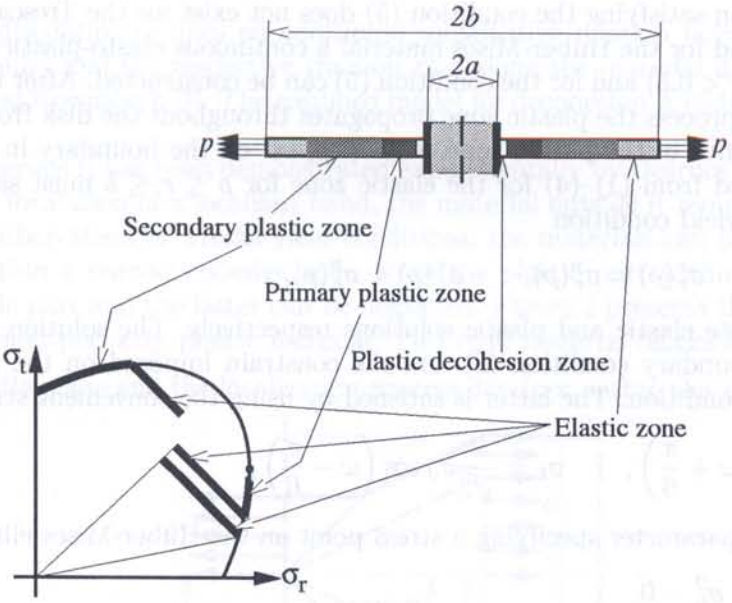

Fig. 1. Zones in the annular disk of elastic-perfectly plastic material

$$\frac{\partial \sigma_r}{\partial r} + \frac{\sigma_r - \sigma_t}{r} = 0, \tag{1}$$

$$\varepsilon_r = \frac{1}{E}(\sigma_r - \nu\sigma_t), \qquad \varepsilon_t = \frac{1}{E}(\sigma_t - \nu\sigma_r), \tag{2}$$

$$\varepsilon_r = \frac{\partial u}{\partial r}, \qquad \varepsilon_t = \frac{u}{r}, \tag{3}$$

where E and ν are elastic constants. The boundary condition for the external edge is specified as

$$\sigma_r(b) = p \tag{4}$$

and at the beginning of the loading process the respective condition for the internal edge is given as

$$u(a) = 0. \tag{5}$$

The onset of plastic flow occurs at $r = a$, when the external pressure exceeds the value:

$$p_T = \frac{\sigma_0}{2b^2}\left[(1+\nu)b^2 + (1-\nu)a^2\right] \qquad \text{for Treska yield condition,}$$

$$p_{HM} = \frac{\sigma_0}{2\sqrt{1-\nu+\nu^2}b^2}\left[(1+\nu)b^2 + (1-\nu)a^2\right] \qquad \text{for Huber-Mises yield condition}$$

(σ_0 is the yield stress).

2.1. Initiation of decohesion

When the first plastic flow occurs for the Tresca material, then $\sigma_r(a) = \sigma_0$ and $\sigma_t(a) < \sigma_0$. It follows from the equilibrium condition, that the stress states within the subsequent plastic regime must satisfy the yield condition $\sigma_t - \sigma_0 = 0$, so the state $\sigma_r(a) = \sigma_t(a) = \sigma_0$ should have been

reached immediately. It is seen, that without the admitted displacement discontinuity at $r = a$ an elasto-plastic solution satisfying the condition (5) does not exist for the Tresca material.

On the other hand for the Huber-Mises material a continuous elasto-plastic solution for a compressible material ($\nu < 0.5$) and for the condition (5) can be constructed. After the first phase of the elastic deformation process the plastic zone propagates throughout the disk from the interior edge. Denote by ρ the radius of the plastic zone. At $r = \rho$, i.e. on the boundary in between two zones, the solution obtained from (1)–(4) for the elastic zone for $\rho \leq r \leq b$ must satisfy the continuity conditions and the yield condition

$$u^e(\rho) = u^p(\rho), \qquad \sigma_r^e(\rho) = \sigma_r^p(\rho), \qquad \sigma_t^e(\rho) = \sigma_t^p(\rho), \tag{6}$$

where e and p denote elastic and plastic solutions respectively. The solution for the plastic zone must satisfy the boundary condition (5) and the constrain imposed on the stress states by the Huber-Mises yield condition. The latter is satisfied by using the convenient stress representation

$$\sigma_r = \frac{2}{\sqrt{3}}\sigma_0 \cos\left(\omega + \frac{\pi}{6}\right), \qquad \sigma_t = \frac{2}{\sqrt{3}}\sigma_0 \cos\left(\omega - \frac{\pi}{6}\right), \tag{7}$$

where ω is a stress parameter specifying a stress point on the Huber-Mises ellipse

$$\sigma_r^2 + \sigma_t^2 - \sigma_r\sigma_t - \sigma_0^2 = 0. \tag{8}$$

Thus, the stress field in the plastic zone for $a \leq r \leq \rho$ is specified by providing a function $\omega = \omega(r)$.

When the associated flow rule is used, the strain and stress rates are related by

$$\left(\dot{\varepsilon}_r - \frac{1}{E}(\dot{\sigma}_r - \nu\dot{\sigma}_t)\right)(2\sigma_t - \sigma_r) = \left(\dot{\varepsilon}_t - \frac{1}{E}(\dot{\sigma}_t - \nu\dot{\sigma}_r)\right)(2\sigma_r - \sigma_t), \tag{9}$$

where $(\dot{})$ denotes differentiation with respect to time parameter η. Using the equations (1)–(3) the following differential equation for the circumferential strain rate can be derived

$$\frac{d\dot{\varepsilon}_t}{d\omega} - \sqrt{3}\dot{\varepsilon}_t = \frac{2\sigma_0\dot{\omega}}{\sqrt{3}}\left(\frac{1}{4G\sin\omega} + \frac{\sin\omega}{3K}\right), \tag{10}$$

where $K = E/3(1-2\nu)$ is the bulk modulus and $G = E/2(1+\nu)$ is the shear modulus. The above equation can be solved numerically, and then the radial strain component can be determined using the compatibility condition

$$\dot{\varepsilon}_r = \frac{\partial(r\dot{\varepsilon}_t)}{\partial r}. \tag{11}$$

It can be found from the last two equations, that the radial strain rate at $r = a$ is given as follows

$$\dot{\varepsilon}_r(a) = \frac{-2\sigma_0\dot{\omega}}{\sqrt{3}\cos\left[\omega(a) - \frac{\pi}{3}\right]}\left(\frac{1}{4G} + \frac{\sin^2\omega(a)}{3K}\right). \tag{12}$$

Note, that the radial strain $\varepsilon_r(a)$ increases rapidly, tending to infinity when the stress point representing the stress state in the plane $\sigma_r - \sigma_t$ for $r = a$ approaches the parabolic point at $\omega = \frac{11}{6}\pi$. Such infinite strain (or a displacement discontinuity) may create doubt about the physical validity of the solution. In fact, this means that a regular elasto-plastic solution no longer exists.

Physically, it can be expected that a localized flow zone occurs in the situation described above. Various physical criteria of decohesion were extensively investigated in the literature. It was found by Clift *et al.* in [8], that among all published continuum fracture criteria the only one, which is in accordance with experiments and successfully predicts the fracture initiation, is a limited value of unit plastic work. In view of this conclusion only limited plastic strains may occur within the discussed annular disk and the onset of decohesion near the edge $r = a$ must occur.

2.2. Simplified constitutive model for decohesion

In the presence of discontinuity lines an additional constitutive relation between the rate of displacement discontinuity and the respective traction rate along the material discontinuity line was assumed by Mróz and Kowalczyk [7]. The assumed model for decohesion is justified by the following reasoning.

For granular materials it has been demonstrated experimentally by Desrues in [9] in plane strain tests, that after the formation of a localized band, the material outside it remains essentially rigid. Similarly, for the Huber-Mises or Treska yield conditions, the materials can be treated as a rigid-perfectly plastic within a narrow cohesive zone, since the plastic part within strain components dominate over elastic part and the latter can be neglected. Figure 2 presents the mode of deformation in the case of rigid-perfectly plastic material. Two rigid material blocks are sliding along slip planes towards middle plane and the localization process develops within the zone $a \leq r \leq a + \frac{H}{2}$.

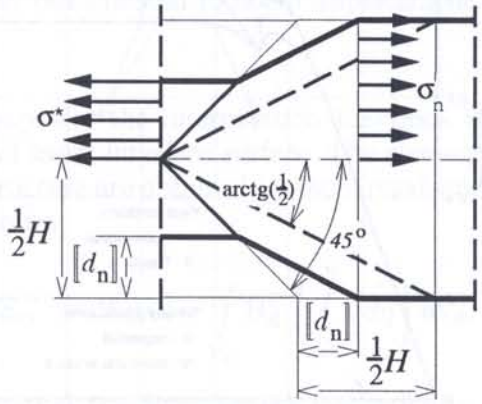

Fig. 2. Mode of deformation in the localized zone.

The inner edge of the disk is displaced by

$$u(a) = [\![d_n]\!] \tag{13}$$

(where $[\![d_n]\!]$ describes displacement jump across plastic decohesion zone). The reduced thickness at this edge is $h = H - 2[\![d_n]\!]$. Within an assumption that the radial stress distribution is uniform, from the condition of equilibrium of radial forces it follows

$$\left.\begin{aligned} \sigma_r(a) &= \sigma^* \left(1 - \frac{2}{H}[\![d_n]\!]\right) \quad \text{for} \quad [\![d_n]\!] < \frac{H}{2} \\ \sigma_r(a) &= 0 \qquad\qquad\qquad\quad \text{for} \quad [\![d_n]\!] \geq \frac{H}{2} \end{aligned}\right\}, \tag{14}$$

where σ^* denotes the radial stress at the onset of decohesion process. On the other hand, the usual flow rule occurs within domains of regular solution. The conditions (13) and (14) replace the boundary condition (5) in the analysis of deformation process in the presence of the progressive decohesion.

The methodology developed by Mróz and Kowalczyk in [7] could be applied to any problem where the localized deformation develops. It was shown, that the separation of disk and hub induces the post-critical behavior of the disk. The continuous solutions for Tresca and Huber-Mises materials were presented thoroughly using the Hencky-Ilyushin deformation theory and for the flow theory. It was shown, that the onset of decohesion within the annular disk may be followed by both stable or unstable response. As was shown in [12] the primary plastic zone is small, so it was neglected in [7] when using the Hencky-Ilyushin deformation theory and only the secondary plastic zone was taken into account. The obtained load-displacement curves for the Treska and Huber-Mises

materials were similar. However, the respective curve obtained using the flow theory and taking into account the primary plastic zone was significantly different (see Fig. 3). The response is also very sensitive on the disk thickness since the decohesive ductility specified by the conditions (13) and (14) depend explicitly on H. In all cases the previous analysis was finished at the limit states with the secondary plastic zone spread over the whole disk. Recalling the conclusion of Clift ([8]) the plastic deformation can not proceed into infinity, so the analysis presented in [7] does not solve the disk problem to the end. It can be expected that the separation from the hub might be followed by the evolution of radial localization zones which subsequently become the radial cracks leading to the ultimate disk collapse.

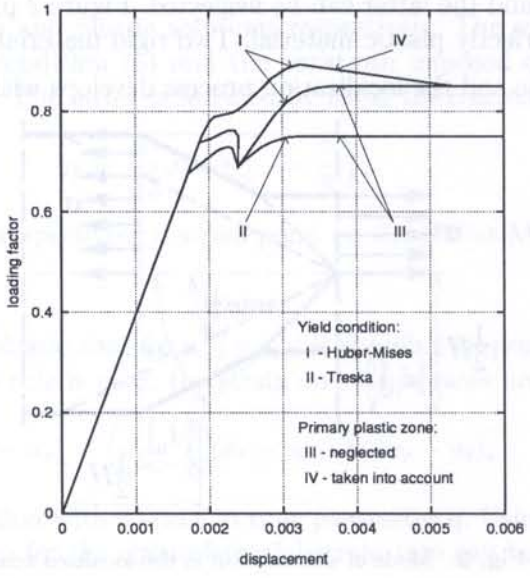

Fig. 3. Response curves of load factor versus displacement.

3. Finite element modeling for nonlinear structure

In this Section a brief outline of the derivation of discrete equations with the aid of finite element method is presented. The general consideration described below should facilitate to assess a meaning of the assumed simplification in the structural modeling. In a sequel the attention is focused on the numerical method used as a solver for boundary value problems.

3.1. Discrete set of equation

The finite element method based on a displacement discretization is used in the paper in order to solve the problems with the interaction of diffuse and localized plasticity. The evolution of these two forms of deformation are described by two different constitutive models implemented into two different types of finite elements. The evolution of diffusive plasticity within domains of material outside the localization zones is described by the classical theory of plasticity, where the strain rates $\dot{\boldsymbol{\varepsilon}}$ are related to the stress rates $\dot{\boldsymbol{\sigma}}$. On the other hand, the constitutive relation used for material within the decohesive cracks describes variation of the tractions rates $\dot{\mathbf{t}}$ with respect to the displacement discontinuity rates $[\![\dot{\mathbf{d}}]\!]$. Below, the differences between two forms of material description are prescribed by the sub-indices c and d. Thus, the respective constitutive equations are given as

$$\dot{\mathbf{t}} = \tilde{\mathbf{D}}_c [\![\dot{\mathbf{d}}]\!], \qquad \dot{\boldsymbol{\sigma}} = \tilde{\mathbf{D}}_d \dot{\boldsymbol{\varepsilon}}, \tag{15}$$

where $\tilde{\mathbf{D}}_c$ denotes the elasto-plastic stiffness matrix for the material within the cracks, while the matrix $\tilde{\mathbf{D}}_d$ describes the diffuse plasticity.

Let M denote the number of unknown nodal displacements $\mathbf{u}$ within the structure. The vector of nodal displacements $\mathbf{u}^e$ within a specific element may be derived from $\mathbf{u}$ by means of the relation

$$\mathbf{u}^e = \mathbf{A}^e \mathbf{u}, \tag{16}$$

with $\mathbf{A}^e$ being known as a Boolean matrix. The rates of displacements and strains at any point within the element, where the diffuse plasticity evolves, are presented in the form

$$\dot{\mathbf{d}} = \mathbf{N}_d \dot{\mathbf{u}}^e, \qquad \dot{\boldsymbol{\varepsilon}} = \mathbf{B}_d \dot{\mathbf{u}}^e, \tag{17}$$

where $\mathbf{N}_d$ and $\mathbf{B}_d$ denote the matrices with the respective interpolation functions. Decohesive cracks are modeled by the interface elements characterized by zero thickness and doubled nodes. The displacement discontinuity rates related to nodal displacement rates are given as follows

$$[\![\dot{\mathbf{d}}]\!] = \mathbf{B}_c \dot{\mathbf{u}}^e. \tag{18}$$

Hereby, the matrix $\mathbf{B}_c$ encompasses the interpolation functions taking into account the nodes, which belong to the upper and lower interface surface. The element internal forces $\mathcal{F}_c$ and $\mathcal{F}_d$ induced within the deformed structure are obtained by the virtual-work method. They are calculated through integration of stress rates

$$\mathcal{F}_c(\mathbf{u}) = \int_{S_c} \mathbf{B}_c^T \left(\int_0^\eta \dot{\mathbf{t}} d\eta \right) dS_c, \qquad \mathcal{F}_d(\mathbf{u}) = \int_{V_d} \mathbf{B}_d^T \left(\int_0^\eta \dot{\boldsymbol{\sigma}} d\eta \right) dV_d. \tag{19}$$

The above relations underline that the displacement discontinuity rates within the interface elements correspond to the classical strain rates, and the most important difference between modeling of diffuse and localized plasticity is hidden within the constitutive equations.

Let us introduce an M-dimensional reference vector $\mathbf{F}$ given as

$$\mathbf{F} = \sum_e \mathbf{A}^{eT} \left[\int_{V^e} \mathbf{N}^{eT} \mathbf{f} dV + \int_{S^e} \mathbf{N}^{eT} \mathbf{p} dS_p \right], \tag{20}$$

where $\mathbf{f}$ and $\mathbf{p}$ denote the prescribed constant body force per unit volume and the prescribed surface tractions, respectively. The summation over the second integral within the brackets is performed if the element boundary S^e constitutes a portion of the loaded surface S_p of the discretized structure. Within the considered problems it is assumed, that the global external forces are proportional to $\mathbf{F}$ scaled by the loading factor λ. The global internal forces $\mathcal{F}$ are obtained as

$$\mathcal{F}(\mathbf{u}) = \sum_e \mathbf{A}^{eT} \mathcal{F}^e(\mathbf{u}), \tag{21}$$

where the element internal forces $\mathcal{F}_c$ and $\mathcal{F}_d$ are now denoted by $\mathcal{F}^e$. In view of continuation methods discussed below it is important to note, that the internal forces are continuously differentiable functions of the nodal displacement vector $\mathbf{u}$. The relation between the nodal displacements and external loading is sought through the equilibrium condition between external and internal forces

$$\mathcal{G}(\mathbf{r}) = \mathcal{F}(\mathbf{u}) - \lambda \mathbf{F} = \mathbf{0}. \tag{22}$$

In the literature, it is natural, that the loading factor is identified with the independent parameter, whereas the displacements constitute dependent variables. Thus, the incremental system is usually presented in the form

$$\mathbf{K} \delta \mathbf{u} = \mathcal{E} + \mathbf{F} \delta \lambda, \tag{23}$$

where $\mathcal{E} = \lambda \mathbf{F} - \mathcal{F}(\mathbf{u})$ denotes the residual nodal forces and the square $(M \times M)$ matrix $\mathbf{K}$ is known as tangent stiffness given as

$$\mathbf{K} = \sum_e \mathbf{A}^{eT} \left[\int_{V^e} \mathbf{B}^{eT} \tilde{\mathbf{D}} \mathbf{B}^e dV \right] \mathbf{A}^e. \tag{24}$$

The details concerning the finite element method and the derivation of equilibrium equations can be found in the literature (see, for example, [14, 15, 17]). Here note, that the equations (22) constitute a particular form of (36) with the vector $\mathbf{r}$ composed of $(M+1)$ state variables $\mathbf{u}$ and λ.

3.2. Diffuse plastic zone

Particular form of the elasto-plastic stiffness matrix $\tilde{\mathbf{D}}_d$ depends on the constitutive relation adopted for the element. Consider additive decomposition

$$\dot{\boldsymbol{\varepsilon}} = \dot{\boldsymbol{\varepsilon}}^e + \dot{\boldsymbol{\varepsilon}}^p, \tag{25}$$

where $\dot{\boldsymbol{\varepsilon}}^e$ and $\dot{\boldsymbol{\varepsilon}}^p$ are elastic and plastic components of strain rate. In the present paper, the elastic stress-strain relation is given by the Hooke's law, while the plastic strain rate follows from the associated flow rule as

$$\dot{\boldsymbol{\sigma}} = \mathbf{D}_d \dot{\boldsymbol{\varepsilon}}^e, \qquad \dot{\boldsymbol{\varepsilon}}^p = \dot{\Lambda}_d \frac{\partial \mathcal{H}_d}{\partial \boldsymbol{\sigma}} \tag{26}$$

where $\dot{\Lambda}_d (\geq 0)$ is the proportionality factor. For the analyzed thin sheet the Huber-Mises yield condition

$$\mathcal{H}_d(\boldsymbol{\sigma}) = \sqrt{3J_2} - \sigma_0 = 0 \tag{27}$$

is considered in the plane stress. Thus, the second invariant of the deviatoric stress tensor is given as $J_2 = \frac{1}{3}(\sigma_{11}^2 - \sigma_{11}\sigma_{22} + \sigma_{22}^2 + 3\sigma_{12}^2)$. The material stiffness matrix $\tilde{\mathbf{D}}_d$ for a perfectly plastic material model is of the form

$$\tilde{\mathbf{D}}_d = \begin{cases} \mathbf{D}_d \left(\mathbf{I} - \dfrac{\left(\dfrac{\partial \mathcal{H}_d}{\partial \boldsymbol{\sigma}}\right)^T \dfrac{\partial \mathcal{H}_d}{\partial \boldsymbol{\sigma}} \mathbf{D}_d}{\dfrac{\partial \mathcal{H}_d}{\partial \boldsymbol{\sigma}} \mathbf{D}_d \left(\dfrac{\partial \mathcal{H}_d}{\partial \boldsymbol{\sigma}}\right)^T} \right) & \text{if} \quad \mathcal{H}_d = 0, \quad \dot{\Lambda}_d > 0, \\ \mathbf{D}_d = \dfrac{E}{1-\nu^2} \begin{bmatrix} 1 & \nu & 0 \\ \nu & 1 & 0 \\ 0 & 0 & \dfrac{1-\nu}{2} \end{bmatrix} & \text{if} \quad \begin{cases} \mathcal{H}_d < 0, & \text{or} \\ \mathcal{H}_d = 0, & \dot{\Lambda}_d \leq 0. \end{cases} \end{cases} \tag{28}$$

In the present paper, the above tangent stiffness matrix was implemented into the simplest 3-node uniform strain elements.

3.3. Localization zones treated as discontinuity interfaces

Denote by $\mathbf{n}$ the normal vector to localization zone. Within the local reference frame defined by $\mathbf{n}$ the constitutive model for decohesive crack may be effectively derived following the classical plasticity theory. First, the additive decomposition is assumed

$$[\![\dot{\mathbf{d}}]\!] = [\![\dot{\mathbf{d}}]\!]^e + [\![\dot{\mathbf{d}}]\!]^p, \tag{29}$$

where the displacement rate discontinuities are expressed as the sum of the elastic (reversible) part $[\![\dot{\mathbf{d}}]\!]^e$ and a plastic (irreversible) one $[\![\dot{\mathbf{d}}]\!]^p$. For the elastic part the constitutive law is assumed as

$$\dot{\mathbf{t}} = \mathbf{D}_c [\![\dot{\mathbf{d}}]\!]^e. \tag{30}$$

Note, that the matrix of elastic stiffnesses $\mathbf{D}_c$ has the dimension of a force per unit length. As there is no adequate experimental data, in practice, $\mathbf{D}_c$ can be taken as diagonal, i.e. coupling between normal and shear tractions can be neglected. Also the unilateral effect can be taken into account using different stiffnesses for tension and compression, i.e. $D_{c11} = E_n^+$ for $t_n > 0$ and $D_{c11} = E_n^-$ for $t_n < 0$, where t_n denotes the normal traction to the decohesive direction. The associate flow rule for plastic displacement rate discontinuities

$$[\![\dot{\mathbf{d}}]\!]^p = \dot{\Lambda}_c \frac{\partial \mathcal{H}_c}{\partial \mathbf{t}} \tag{31}$$

is obtained using the interface yield condition

$$\mathcal{H}_c(\mathbf{t}, [\![\mathbf{d}]\!]^p) \leq 0, \tag{32}$$

where $\dot{\Lambda}_c \geq 0$ denotes the scalar parameter. Herein, $\mathcal{H}_c$ depends on the plastic part of displacement discontinuities taken as damage variables. It can be found using the compatibility condition

$$\frac{\partial \mathcal{H}_c}{\partial [\![\mathbf{d}]\!]^p} [\![\dot{\mathbf{d}}]\!]^p + \frac{\partial \mathcal{H}_c}{\partial \mathbf{t}} \dot{\mathbf{t}} = 0 \tag{33}$$

that the elasto-plastic tangent stiffness matrix for the interface material is given as

$$\tilde{\mathbf{D}}_c = \begin{cases} \mathbf{D}_c \left(\mathbf{I} - \dfrac{\left(\dfrac{\partial \mathcal{H}_c}{\partial \mathbf{t}}\right)^T \dfrac{\partial \mathcal{H}_c}{\partial \mathbf{t}} \mathbf{D}_c}{L_c + \dfrac{\partial \mathcal{H}_c}{\partial \mathbf{t}} \mathbf{D}_c \left(\dfrac{\partial \mathcal{H}_c}{\partial \mathbf{t}}\right)^T} \right) & \text{if} \quad \mathcal{H}_c = 0, \quad \dot{\Lambda}_c > 0, \\ \mathbf{D}_c = \begin{bmatrix} D_{c11} & 0 \\ 0 & D_{c22} \end{bmatrix} & \text{if} \begin{cases} \mathcal{H}_c < 0, & \text{or} \\ \mathcal{H}_c = 0, \ \dot{\Lambda}_c \leq 0. \end{cases} \end{cases} \tag{34}$$

where $L_c = -\dfrac{\partial \mathcal{H}_c}{\partial [\![\mathbf{d}]\!]^p} \left(\dfrac{\partial \mathcal{H}_c}{\partial \mathbf{t}}\right)^T$ is the hardening modulus for the interface material. The constitutive model derived from the general scheme presented above may render the main characteristic necessary to the modeling the decohesive crack evolution: the unilateral effects, irreversible deformation and anisotropic damage.

3.4. Onset of localization and Rankine's criterion

One of the crucial aspects of decohesion is the onset of localization. There is extensive literature devoted to hardening and softening materials, where in general decohesion is considered as a phenomenon resulting from the bifurcation of equilibrium states within diffuse plastic zone. The onset of discontinuous localization takes place when the so-called acoustic tensor is singular, i.e. there exists a solution to the eigenvalue problem

$$\mathbf{Q}\,\mathbf{c} = \left(\mathbf{n}\tilde{\mathbf{D}}_d\mathbf{n}\right)\mathbf{c} = \mathbf{0} \tag{35}$$

where $\mathbf{c}$ determines the mode of deformation. For associative plasticity and for plane stress, it can be shown (see [11, 10]), that the bifurcation may occur only for zero hardening modulus. However, the preliminary example indicates that decohesion may also occur within the elastic-perfectly plastic structure as a result of inadmissible infinite increase of normal strain. In such a case the post-critical states within the structure are described by unique solution.

For the tests on the new numerical method described below even simple discretization, which renders the main physical aspects of interaction between diffuse and localized plasticity, are satisfactory. For the same reason the analysis of the acoustic tensor is abandoned. It is assumed, that the decohesion proceeds if the respective loading condition within the localization zone is satisfied. Once a decohesion starts to evolve, no matter whether this occurs within material which exhibits hardening or perfect plasticity, the overall behavior is governed by the behavior within the band.

The interface elements and the material response used in the present paper are presented in Fig. 4. The 4-node interface elements with initial zero thickness were used for modeling the decohesive cracks. The tangential discontinuity is neglected and only opening mode is studied. Thus, the cracks evolve when the stresses attain a limit strength curve corresponding to Rankine's criterion: the resistance of the material is limited to its uniaxial tensile strength σ_0. To avoid penetration of the interface element into the adjacent material, the compressive interface modulus E_n^- is assumed much larger then the tensile modulus E_n^+. The first phase of the process (for $\sigma_n \in [0, \sigma_0]$ and $[\![d_n]\!] = 0$) is approximated by a penalty function, so the decohesion starts for $[\![d_n]\!] = [\![d_{n1}]\!]$. When $[\![d_n]\!] > [\![d_{n2}]\!]$, the normal stress vanishes and the interface opening occurs.

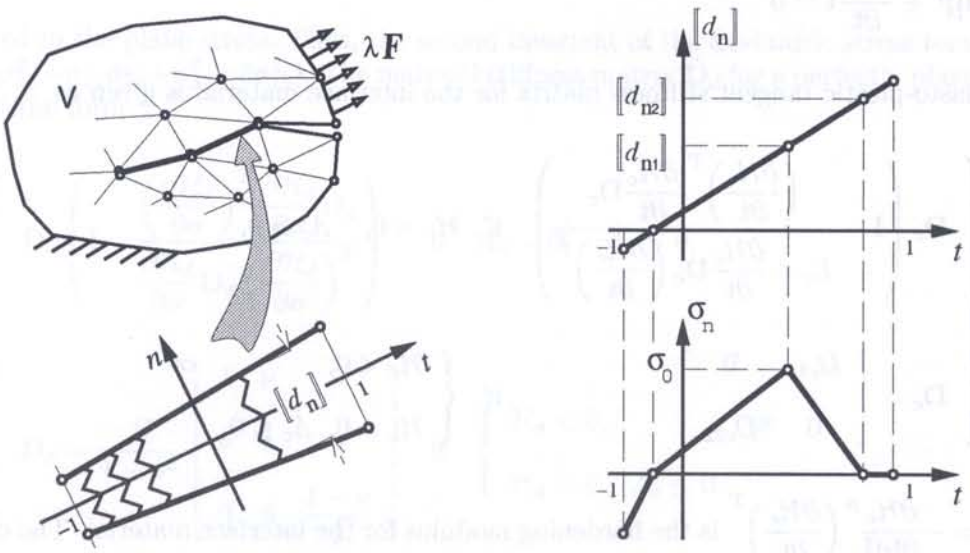

Fig. 4. Discretization and material characteristic within interface element.

4. INCREMENTAL-ITERATIVE APPROACH TO NONLINEAR PROBLEMS

Let us briefly describe a general framework of continuation methods in order to underline the similarities and distinctions between the well known schemes and the control variable selection method presented in the subsequent Section. Consider a nonlinear problem defined by a set of equations

$$\mathcal{G}(\mathbf{r}) = \mathbf{0} \tag{36}$$

with $\mathbf{r}$ being the vector of N state variables r_i $(i = 1, \ldots, N)$ and $\mathcal{G}$ denoting the vector field specified by $M = N - 1$ real functions $\mathcal{G}_m(\mathbf{r})$ $(m = 1, \ldots, M)$. The solution set of the problem (36) constitutes a manifold. Using continuation techniques, the shape of this manifold is revealed by a series of points R_i. The sub-indices $i = 0, 1, \ldots$ establish a connectivity among the determined points. Calculations begin from a known solution point R_0 and the coordinates of the consecutive points R_i satisfy the relation

$$\mathbf{r}_{\omega+1} = \mathbf{r}_\omega + \Delta\mathbf{r}_\omega = \mathbf{r}_0 + \sum_{i=0}^{\omega} \Delta\mathbf{r}_i. \tag{37}$$

The increments $\Delta\mathbf{r}_\omega$ are obtained from a series of sub-increments $\delta\mathbf{r}^\nu$. Among any two solution points, say R_ω and $R_{\omega+1}$, a series of the approximating points R^ν (for $\nu = 0, 1, \ldots$) are established. The coordinates of two consecutive points R^ν and $R^{\nu+1}$ are related as

$$\mathbf{r}^{\nu+1} = \mathbf{r}^\nu + \delta\mathbf{r}^\nu. \tag{38}$$

Denote the difference between $\mathbf{r}^\nu$ and $\mathbf{r}^0$ as the increment $\Delta\mathbf{r}^\nu$. This increment can be presented as follows

$$\Delta\mathbf{r}^\nu = \mathbf{r}^\nu - \mathbf{r}^0 = \begin{cases} \mathbf{0} & \text{for} \quad \nu = 0 \\ \displaystyle\sum_{j=0}^{\nu-1} \delta\mathbf{r}^j & \text{for} \quad \nu > 0. \end{cases} \tag{39}$$

In a predictor step (for $\nu = 0$), the last determined point is taken as an initial approximation, i.e. $R^0 \equiv R_\omega$. The vector $\mathbf{r}^0 = \mathbf{r}_\omega$ and the initial sub-increment $\delta\mathbf{r}^0$ establish the first approximation R^1, which usually does not satisfy the equation (36). The solution has to be improved iteratively during a corrector step (for $\nu > 0$). If the iteration proceeds successfully, then the increments $\Delta\mathbf{r}^\nu$ converge to the sought increment $\Delta\mathbf{r}_\omega$. The convergence means that $\lim_{\nu\to\infty} \|\mathcal{E}\| = 0$ (here $\|(\cdot)\|$ denotes the Euclidean vector norm and $\mathcal{E} = -\mathcal{G}(\mathbf{r}^\nu)$).

The calculation can not be endless, so in practice, the process is terminated in three basic cases:

1. if $\|\mathcal{E}\| < \varepsilon$, i.e. the specified numerical tolerance ε is achieved;
2. if $\nu > \nu_{\max}$, i.e. the number of iterations exceeds the specified maximum $\nu_{\max}$;
3. if $\Delta\mathbf{r}^{\nu+1} \approx \Delta\mathbf{r}^\nu$, i.e. the sub-increment $\delta\mathbf{r}^\nu$ is too small.

In the first case, the sought solution point is identified with the last approximation, i.e. $R^\nu = R_{\omega+1}$. In the second case, the convergence is too slow or the iteration diverges. Usually, the predictor step has to be repeated with the shorter step length $\|\Delta\mathbf{r}^1\|$. The third case can be caused, for example, due to confined representation of numbers in computers. More details concerning the step length adjustment and termination problem can be found in Seydel [13] or Crisfield [14].

The sub-increments $\delta\mathbf{r}^{\nu}$ are calculated from an augmented incremental system composed of the linearized form of the system (36) and the constraint equation. The linearized incremental system can be obtained from a Taylor series expansion

$$\mathcal{G}(\mathbf{r}^{\nu+1}) = \mathcal{G}(\mathbf{r}^{\nu}) + \left.\frac{\partial \mathcal{G}}{\partial \mathbf{r}}\right|_{\mathbf{r}}^{\nu} \delta\mathbf{r}^{\nu} + \Theta \tag{40}$$

(here Θ denotes the sum of higher order terms). Using two assumptions

$$\mathcal{G}(\mathbf{r}^{\nu+1}) \approx \mathbf{0}, \qquad \Theta \approx \mathbf{0} \tag{41}$$

the linear truncated form is achieved

$$\mathbf{G}\delta\mathbf{r}^{\nu} = \mathcal{E}, \tag{42}$$

where $\mathbf{G}$ denotes the $(M \times N)$ rectangular matrix with the rows composed of gradients $\mathbf{g}_m = \partial\mathcal{G}/\partial\mathbf{r}|_{\mathbf{r}}^{\nu}$. For $\nu = 0$, the entries of $\mathcal{E}$ are negligible small, so the system (42) can be treated as homogeneous

$$\mathbf{G}\delta\mathbf{r}^{0} = \mathbf{0} \tag{43}$$

but, for $\nu > 0$, the system (42) is non-homogeneous and it has more unknowns then equations. Additional linearly independent equation is required in order to calculate the sought vector $\delta\mathbf{r}^{\nu}$. The incremental system is augmented by a so-called constraint equation.

There is no physical prerequisites for constraint equation, so a great variety of continuation schemes can be found in the literature. The well known methods relay on some arbitrarily assumed physical or geometrical conditions. For example, the Newton-Raphson method at a fixed load level has been used in [20], the work-increment control in [21] and the arc-length control in [22, 23, 24]. The constraint equation is used in the explicit form, which can be presented as follows

$$\mathbf{g}_N \delta\mathbf{r}^{\nu} = \begin{cases} \Delta\eta_{\omega} & \text{for } \nu = 0, \\ 0 & \text{for } \nu > 0, \end{cases} \tag{44}$$

where $\mathbf{g}_N$ is the vector of assumed coefficients and $\Delta\eta_{\omega}$ denotes the prescribed increment. The path parameter is switched from η_{ω} to $\eta_{\omega+1} = \eta_{\omega} + \Delta\eta_{\omega}$ at predictor step (for $\nu = 0$), and it remains unchanged during subsequent iteration at corrector step (for $\nu > 0$). The pictures shown in Fig. 5 are widely used in the literature in order to visualize the well known continuation schemes.

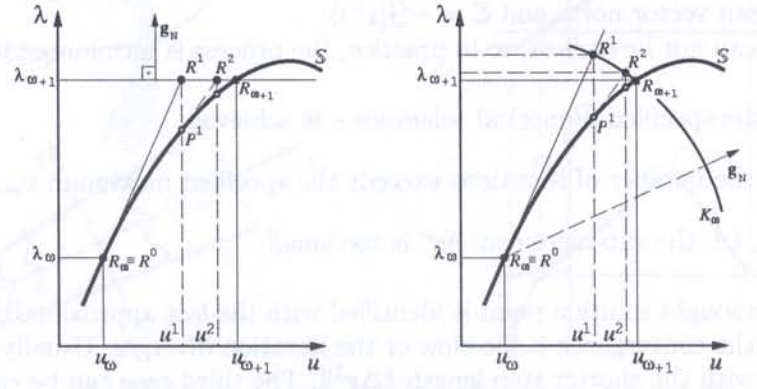

Fig. 5. Graphical interpretation of continuation schemes: a) Newton-Raphson method at a fixed load level, b) spherical method.

5. Control variable selection method

The new compatible continuation method (cf. [18, 19]) is based on the incremental system (42) rewritten in the form

$$\mathbf{G}\mathbf{x}^* - \mathcal{E}x^*_{N+1} = \mathbf{0}, \tag{45a}$$

$$x^*_{N+1} = 1, \tag{45b}$$

with the simplified notation $\mathbf{x}^* \equiv \delta\mathbf{r}^\nu$ for $\nu = 0, 1, \ldots$. The constraint equation is not prescribed explicitly. The equation (44) is recalled in a sequel only, when an idea of linear superposition of the ultimate correction sub-increment is introduced. The crucial features of the control variable selection method arise from the following obvious observations.

The auxiliary equation (45b) constitutes the scaling condition for an arbitrary vector $\tilde{\mathbf{x}} = \{\mathbf{x}, x_{N+1}\}$, which satisfies the homogeneous system

$$\tilde{\mathbf{A}}_1\tilde{\mathbf{x}} = \mathbf{0} \tag{46}$$

with $\tilde{\mathbf{A}}_1 = [\mathbf{G}, -\mathcal{E}]$. Indeed, if $\tilde{\mathbf{x}}$ constitutes a solution to (46), then the vector $\tilde{\mathbf{x}}^* = \kappa\tilde{\mathbf{x}}$ (with κ being a scalar parameter) also satisfies (46). In particular case, $\tilde{\mathbf{x}}^* \equiv \{\mathbf{x}^*, 1\}$ contains the solution to (42). The equality $x^*_{N+1} = 1$ implies $\mathbf{x}^* = \mathbf{x}/x_{N+1}$ for any known $\tilde{\mathbf{x}}$. The solution vector $\tilde{\mathbf{x}}^*$ (or $\tilde{\mathbf{x}}$) belongs to a nullspace $\mathcal{N}(\tilde{\mathbf{A}}_1)$. Any basis of the nullspace consists of the vectors $\tilde{\mathbf{x}}_\alpha$ for $\alpha = 1, \ldots, K$, where $K = N - \rho + 1$ and $\rho = \mathrm{rank}\tilde{\mathbf{A}}_1$. Taking into account the size of $\tilde{\mathbf{A}}_1$, the inequality $\rho \leq M$ holds true, so at least two distinct vectors $\tilde{\mathbf{x}}_\alpha$ exist. Further, the nontrivial solution to (46) exists and it is not unique. Any solution to (45) can be presented in the form of linear combination

$$\mathbf{x}^* = \sum_{\alpha=1}^{K} e_\alpha \mathbf{x}_\alpha, \tag{47a}$$

$$x^*_{N+1} = \sum_{\alpha=1}^{K} e_\alpha x_{\alpha N+1}, \tag{47b}$$

where e_α denote the coefficients of linear dependence. The incompatibility of the system (42) can be detected, if $x_{\alpha N+1} = 0$ for $\alpha = 1, \ldots, K$.

The control variable selection method splits the incremental procedure into two parts. In the first part, basic solutions to the homogeneous system (46) are determined. In the second part, the vectors $\mathbf{x}_\alpha$ scaled by the coefficients e_α are used in (47) in order to determine the ultimate sub-increment $\delta\mathbf{r}^\nu$.

5.1. Gaussian elimination applied to homogeneous system

The solution vector $\tilde{\mathbf{x}}$ consists of dependent and independent parts denoted by $\tilde{\mathbf{u}}$ and $\tilde{\mathbf{p}}$, respectively. They can be revealed by the Gaussian decomposition with pivoting performed on $\tilde{\mathbf{A}}_1$. The decomposition procedure can be presented in the form

$$\tilde{\mathbf{L}}_n\tilde{\mathbf{A}}_{n+1} = \mathbf{\Pi}^r_n\tilde{\mathbf{A}}_n\mathbf{\Pi}^c_n, \qquad n = 1, 2, \ldots, \tag{48}$$

where n denotes the number of Gaussian transformations successfully accomplished, and $\mathbf{\Pi}^c_n$ and $\mathbf{\Pi}^r_n$ denote the matrices of column and row permutation, respectively. The matrices $\tilde{\mathbf{L}}_n$ and $\tilde{\mathbf{A}}_{n+1}$ have characteristic structure

$$\tilde{\mathbf{L}}_n = \begin{bmatrix} (\tilde{\mathbf{L}}_{11})_n & \mathbf{0} \\ (\tilde{\mathbf{L}}_{21})_n & \mathbf{I}_{M-n} \end{bmatrix}, \qquad \tilde{\mathbf{A}}_{n+1} = \begin{bmatrix} \tilde{\mathbf{U}}_{n+1} & \tilde{\mathbf{P}}_{n+1} \\ \mathbf{0} & \tilde{\mathbf{Q}}_{n+1} \end{bmatrix}, \tag{49}$$

where the important sub-matrices, $(\tilde{\mathbf{L}}_{11})_n$ and $\tilde{\mathbf{U}}_{n+1}$, are the $(n \times n)$ lower unit triangular and the $(n \times n)$ upper triangular. The sub-matrices $\tilde{\mathbf{P}}_{n+1}$, $\tilde{\mathbf{Q}}_{n+1}$ and the identity matrix $\mathbf{I}_{M-n}$ have decreasing dimensions $(n \times N-n+1)$, $(M-n \times N-n+1)$ and $(M-n \times M-n)$, respectively. The decomposition is terminated for $n = M-1$ or, whenever the subsequent pivot $\max_{p,q} \text{abs}(\tilde{Q}_{pq})_n$ (for $p = 1, \ldots, M-n$ and $q = 1, \ldots, N-n+1$) is in the order of relative machine precision. The estimator of condition numbers proposed in [27] can be easily calculated for the matrices $\mathbf{C}_n$ defined in the form

$$\mathbf{C}_n = (\tilde{\mathbf{L}}_{11})_n \tilde{\mathbf{U}}_{n+1}. \tag{50}$$

It is assumed, that the rank of $\tilde{\mathbf{A}}_1$ can be detected using the following rules

$$\rho = \begin{cases} n & \text{if} \quad \text{cond } \mathbf{C}_n < \chi_t, \quad \text{and} \quad \text{cond } \mathbf{C}_{n+1} \geq \chi_t, \\ M & \text{if} \quad \text{cond } \mathbf{C}_M < \chi_t, \end{cases} \tag{51}$$

where χ_t denotes a threshold value.

After decomposition, the non-homogeneous system can be automatically derived in the form

$$\tilde{\mathbf{U}}_{\rho+1} \tilde{\mathbf{u}} = -\tilde{\mathbf{P}}_{\rho+1} \tilde{\mathbf{p}}. \tag{52}$$

The dependent vector $\tilde{\mathbf{u}}$ is uniquely determined by the above system for any independent vector $\tilde{\mathbf{p}}$. Let $\mathbf{i}_\alpha$ denote α-th column of $(K \times K)$ identity matrix $\mathbf{I}_K$. Using an assumption $\tilde{\mathbf{p}} = \mathbf{i}_\alpha$, the solution vectors $\tilde{\mathbf{x}}_\alpha$ are given in the form

$$\tilde{\mathbf{z}}_\alpha = \{\tilde{\mathbf{u}}_\alpha, \mathbf{i}_\alpha\} \Rightarrow \tilde{\mathbf{x}}_\alpha = \mathbf{\Pi}_1^c \ldots \mathbf{\Pi}_\rho^c \frac{\tilde{\mathbf{z}}_\alpha}{\|\tilde{\mathbf{z}}_\alpha\|}. \tag{53}$$

Herein, the vectors $\tilde{\mathbf{x}}_\alpha$ are normalized to unit length, but any other normalization can also be utilized.

In a sequel, it is assumed for simplicity, that the matrix $\mathbf{G}$ has full rank $\rho = M = N-1$ in both steps, predictor and corrector. Thus, $K = 2$ and two basic solutions $\tilde{\mathbf{x}}_1$ and $\tilde{\mathbf{x}}_2$ can be uniquely determined from (52) and (53). The purpose of the first part of control variable selection algorithm is to determine these two vectors.

The above presented Gaussian elimination procedure is not very effective, as it does not exploit all the information which comes from knowing the structure of the underlying problems. In the case of nonlinear mechanical problems, the symmetry and bandness of the tangent stiffness matrix is not utilized. If these two features are taken into account and $\mathbf{K}$ is nonsingular, then the block elimination algorithm (A.2) is much more efficient. The latter reveals a basis in the form

$$\mathbf{C}_M \equiv \mathbf{K} \quad \Rightarrow \quad \begin{cases} \tilde{\mathbf{x}}_1 = [\mathbf{e}, 0, 1] \\ \tilde{\mathbf{x}}_2 = [\mathbf{f}, 1, 0] \end{cases} \tag{54}$$

In the case of ill-conditioned stiffness matrices, the numerical accuracy of the above two vectors is doubtful. The block elimination algorithm (A.2) can not be utilized whenever $\det \mathbf{K} = 0$.

5.2. Sub-increments obtained by linear superposition

Any effective algorithm, which provide a specific basis of the nullspace $\mathcal{N}(\tilde{\mathbf{A}}_1)$, can be used in the first part of control variable selection method. During the second part of the algorithm the ultimate sub-increment $\delta \mathbf{r}^\nu$ is determined by linear superposition (47), while the idea of constraint equation is abandoned.

At predictor step, the vector $\mathcal{E}$ has to be moved into $\tilde{\mathbf{P}}_{M+1}$ in (52), as the nonsingular matrix $\mathbf{C}_M$ can not contain columns composed of zeroes. As a result, the auxiliary variable x_{N+1} is assigned to the entries of $\tilde{\mathbf{p}}$. The second free parameter in $\tilde{\mathbf{p}}$ and the respective column of $\tilde{\mathbf{P}}_{M+1}$ are revealed after the decomposition performed on the rectangular matrix $\mathbf{G}$. Regardless of the problem, which state variable is selected as a second free parameter, two basic solutions to (46) can be anticipated in the form $\tilde{\mathbf{x}}_1 = \{\mathbf{0}, 1\}$ and $\tilde{\mathbf{x}}_2 = \{\mathbf{x}_2, 0\}$. It is seen, that $\|\delta\mathbf{r}^0\| = e_2$ (because $\|\tilde{\mathbf{x}}_2\| = \|\mathbf{x}_2\| = 1$), whereas e_1 does not influence the vector $\delta\mathbf{r}^0$. The ultimate vector obtained from (47) is given in the form $\delta\mathbf{r}^0 = e_2\mathbf{x}_2$. Only the length of initial sub-increment has to be established and this assures the consistency at predictor step.

At corrector step all columns of $\mathbf{G}$ and the nonzero vector $\mathcal{E}$ are subjected to Gaussian transformations (48). In such a case, the values $x_{1_{N+1}}$, $x_{2_{N+1}}$ can not be predicted in advance ($\|\tilde{\mathbf{x}}_\alpha\| = \|\mathbf{x}_\alpha\| = 1 \Rightarrow x_{\alpha_{N+1}} \in (-1, 1)$). These two numbers influence a freedom in selection of the coefficients e_1, e_2 in the relations (47). Following the idea of constraint equation, the coefficients e_1, e_2 could be determined from the following system

$$\mathbf{g}_N\mathbf{x}_1 e_1 + \mathbf{g}_N\mathbf{x}_2 e_2 = 0, \tag{55a}$$

$$x_{1_{N+1}} e_1 + x_{2_{N+1}} e_2 = 1. \tag{55b}$$

The first equation is obtained using (47a) together with the constraint equation (44), whereas the second follows from (45b) and (47b). Note, that the vector $\mathbf{g}_N$ is used only for the calculation of two scalar products in (55a), i.e. $\mathbf{g}_N\mathbf{x}_1$ and $\mathbf{g}_N\mathbf{x}_2$. Thus, instead of the explicitly assumed entries of $\mathbf{g}_N$, simply two numbers q_1, q_2 can be selected, and the system (55) can be rewritten in the form

$$q_1 e_1 + q_2 e_2 = 0, \tag{56a}$$

$$x_{1_{N+1}} e_1 + x_{2_{N+1}} e_2 = 1. \tag{56b}$$

Such an assumption means, that the vector $\mathbf{g}_N$ does not depend on $\delta\mathbf{r}^\nu$ and the constraint equation (55a) is linear. The consistency of correction method requires, that a determinant of the system (56) should be non-zero. It is seen, that this condition can be easily satisfied in all cases, whenever the inequality $x^2_{1_{N+1}} + x^2_{2_{N+1}} > 0$ holds true. The values of two unknowns e_1, e_2 are given as follows

$$e_1 = \frac{-q_2}{q_1 x_{2_{N+1}} - q_2 x_{1_{N+1}}}, \qquad e_2 = \frac{q_1}{q_1 x_{2_{N+1}} - q_2 x_{1_{N+1}}}. \tag{57}$$

The simplest method arises from an assumption $q_\alpha = \delta_{\alpha\beta}$, where $\delta_{\alpha\beta}$ denotes Kronecker's delta. The subindex β is selected in such a way, that the inequality $x_{\beta_{N+1}} \neq 0$ holds true, so $\mathbf{x}^* = \mathbf{x}_\beta / x_{\beta_{N+1}}$.

The step-length $\|\Delta\mathbf{r}_\omega\|$ between two consecutive solution points, $\mathbf{r}_\omega$ and $\mathbf{r}_{\omega+1}$, is initialized at predictor as $\|\Delta\mathbf{r}^1\| = \|\delta\mathbf{r}^0\| = \Delta s$, and it is not directly controlled during corrector step. The final value $\|\Delta\mathbf{r}_\omega\| = \|\Delta\mathbf{r}^\nu\|$ results from the sum of all consecutive sub-increments $\delta\mathbf{r}^\nu$ for $\nu = 0, 1, \ldots$. The variation of the step length $\Delta s\,(> 0)$ is controlled by some input data and the step-length algorithm, which have been described briefly in [19].

6. Numerical examples

Several problems were solved successfully using a program based on the new continuation algorithm. The solver does not exploit yet all the informations which come from knowing the structure of the underlying incremental homogeneous system, like bandness and symmetry of the tangent stiffness matrix. This confines the size of examples, which can be solved. Nevertheless, the important physical aspects of the decohesion process within thin sheets can be assessed. The numerical examples included below illustrate also characteristic features of the new solution approach. The following sheet thickness and material parameters were assumed: $H = 0.001$ m, $E = 2.1 \times 10^5$ MPa, $\sigma_0 = 500$ MPa, $\nu = 0.3$.

6.1. Circular disk

As a first example, the circular disks were considered with free inner edge $r = a$ and the tensile traction $p = \lambda\sigma_0$ applied at the outer edge $r = b$ (see Fig. 6a). The localization zones modeled as a thin interface were assumed to follow the radial lines. The effect of number c of localization zones has been studied for $a = 0.05$ m, $b = 0.09$ m. In view of symmetry condition, only a half of the portion of disk between two cracks was analyzed. Figure 7a presents a typical mesh addopted in the performed calculations (here, $c = 4$). The propagating radial crack was simulated by seven interface elements placed on the line BC, while the nodes on radial line AD modeled the symmetry axis.

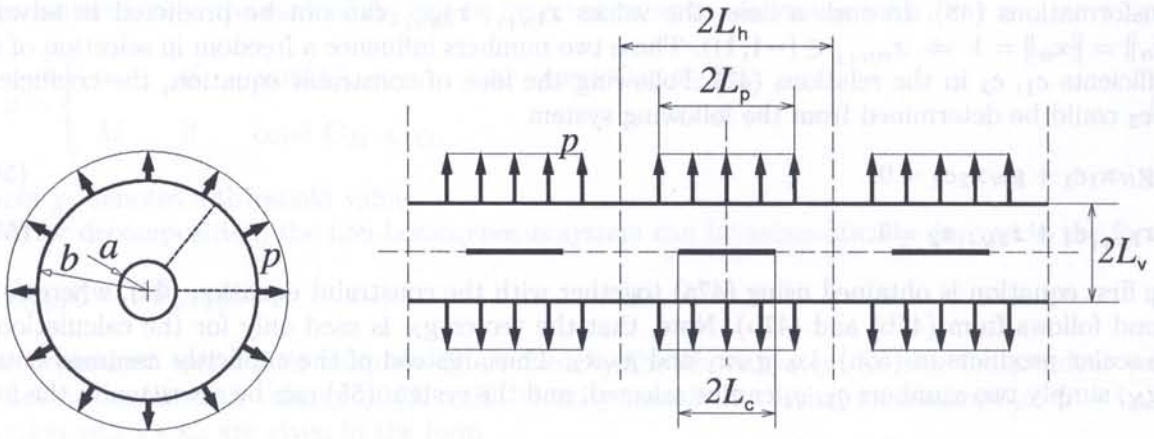

Fig. 6. a) Circular disk, b) Infinite strip with periodic initial cracks.

The numbered nodes in Fig. 7a correspond to the degrees of freedom automatically prescribed as control variables. It is evident, that the solution algorithm selects the control variables, which have an important physical meaning within the considered problem. The selection follows the evolution of propagating crack along the line BC and, in fact, the process is controlled by the displacements near the tip of the crack. The pattern composed by numbered nodes is typical for the considered problem.

The variation of condition numbers of the selected matrix $\mathbf{C}_\rho$ and the tangent stiffness matrix $\mathbf{K}$ versus integration step number are presented in Fig. 7b for $c = 4$. These two curves allow to assess the numerical quality of the obtained results. It is seen, that the algorithm is numerically stable during the whole calculation process as the condition number cond $\mathbf{C}_\rho$ remains on approximately the same level. However, in the case of circular disk, the selected matrix is better conditioned then the stiffness matrix only near the load limit point and at the end of the process, when the crack approaches the outer edge and the stiffness matrix becomes numerically singular. This means, that the utilized Gaussian elimination with complete pivoting does not guarantee, that the matrix $\mathbf{C}_\rho$ attains the possibly lowest condition number among all square matrices of the same size embedded in the rectangular matrix of the homogeneous incremental system.

Figure 8a presents some of the consecutive configurations of the deformed disk contour (the displacements are multiplied by 50). It is seen, that the radial displacements near symmetry axis are higher than near the radial crack. The diffuse plastic zone starts to evolve near the inner edge AB before the load limit point is passed. Within the coarse mesh utilized, only the first layer of elements were plastified, while the remaining portion of the disk remained elastic during the whole deformation process. For the assumed geometrical data the diffuse plasticity did not influenced considerably the ultimate displacements. The differences in radial displacements decrease at the end of the crack evolution, when the external loading is reduced to zero.

The configurations varied similarly for all analyzed crack numbers. Figure 8b presents the effect of number c of localization zones on the response curve of load factor versus displacement of the

node lying on the outer disk edge and symmetry axis (point D in Fig. 7a). As it is seen, when the number c of localization zones increases, the required load level and displacements are higher. For convenience, the results for elastic-perfectly plastic disk without decohesion are also presented. It is seen, that such a case the maximal load level is overestimated.

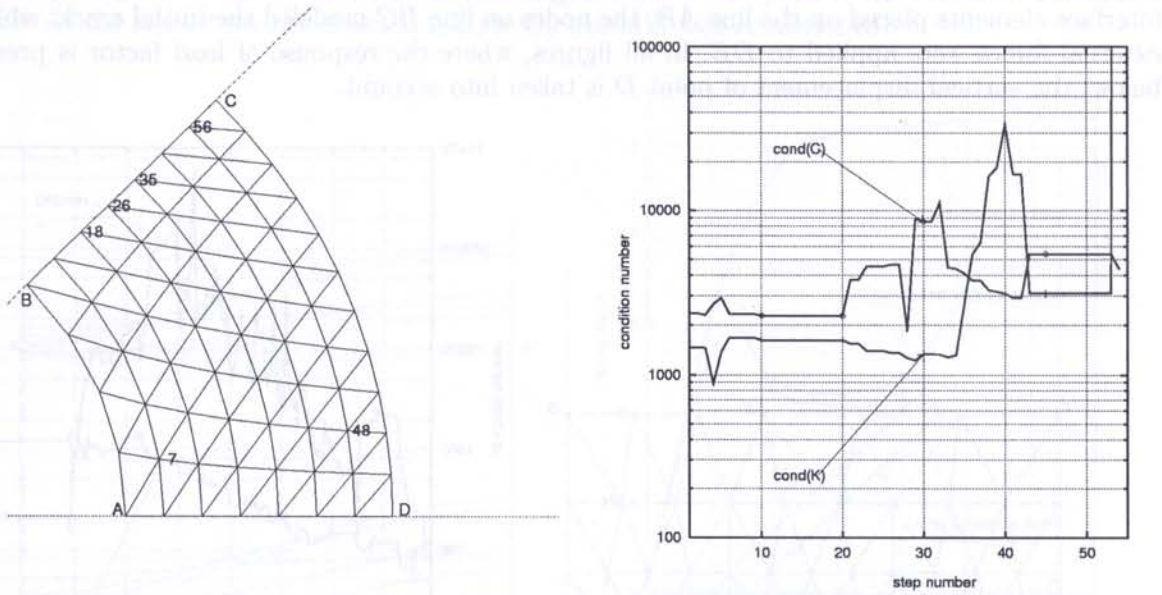

Fig. 7. a) FEM mesh (numbered nodes are those, at which control parameters were selected), b) Condition number versus integration step number; $c = 4$.

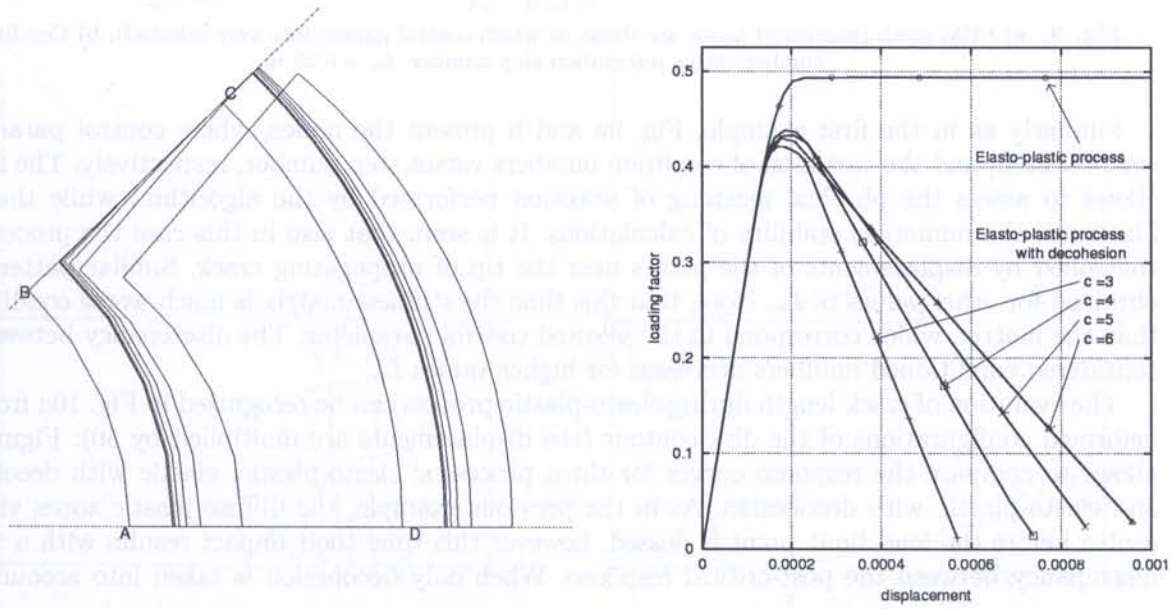

Fig. 8. a) Consecutive contour configurations for $c = 4$, b) Effect of number c of cracks on response curve of load factor versus displacement.

6.2. Infinite strip with periodic initial cracks

As a second example, the infinite strips with periodic initial cracks and periodically distributed tensile traction $p = \lambda\sigma_0$ applied on both sides of the sheet were analyzed (see Fig. 6b). The

localization zones were assumed to develop between the tips of two neighboring initial cracks. In view of symmetry condition, only a quarter of each section was modeled and the effect of the height L_v was studied. The horizontal length L_h, the initial crack length L_c and the length of loaded edge L_p were assumed: $L_h = 0.5$ m, $L_c = 0.1$ m, $L_p = 0.2$ m. Figure 9a presents a typical mesh adopted in the performed calculations (here, $L_v = 0.25$). The crack was simulated by fifteen interface elements placed on the line AB, the nodes on line BC modeled the initial crack, while the external forces were applied to DE. In all figures, where the response of load factor is presented below, the vertical displacement of point D is taken into account.

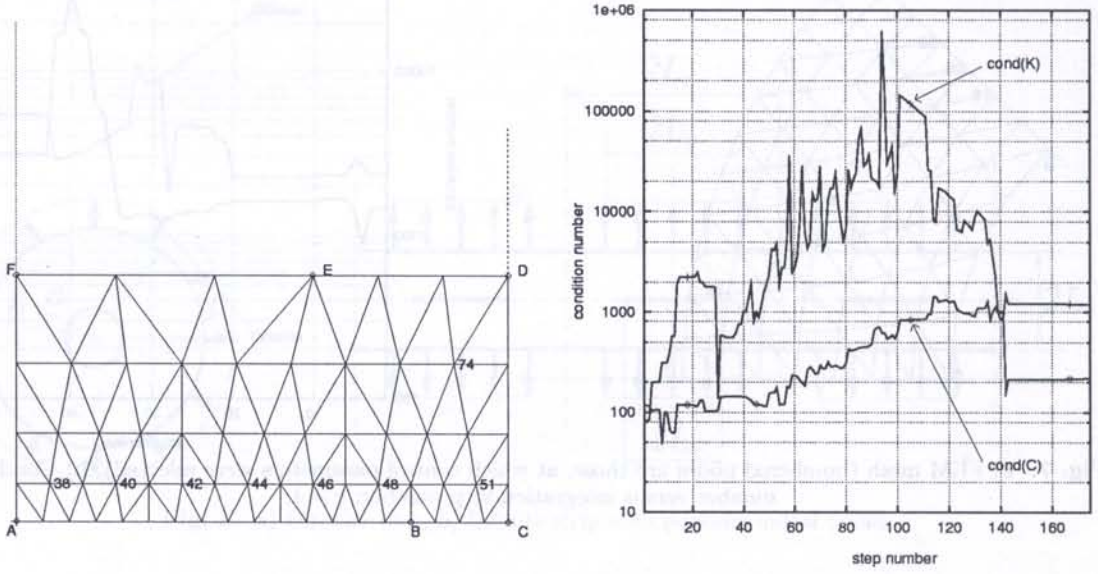

Fig. 9. a) FEM mesh (numbered nodes are those, at which control parameters were selected), b) Condition number versus integration step number; $L_v = 0.25$ m.

Similarly as in the first example, Fig. 9a and b present the nodes, where control parameters were selected, and the variation of condition numbers versus step number, respectively. The former allows to assess the physical meaning of selection performed by the algorithm, while the later illustrates the numerical stability of calculations. It is seen, that also in this case the process was controlled by displacements of the points near the tip of propagating crack. Similar pattern was obtained for other values of L_v. Note, that this time the stiffness matrix is much worse conditioned than the matrix, which correspond to the selected control parameter. The discrepancy between the considered conditioned numbers decreases for higher values L_v.

The evolution of crack length during elasto-plastic process can be recognized in Fig. 10a from the deformed configurations of the disk contour (the displacements are multiplied by 50). Figure 10b allows to compare the response curves for three processes: elasto-plastic, elastic with decohesion and elasto-plastic with decohesion. As in the previous example, the diffuse plastic zones start to evolve before the load limit point is passed, however this time their impact results with a visible discrepancy between the post-critical response. When only decohesion is taken into account, the final displacement is equal $\frac{1}{2}H$ (as a result of the adopted interface constitutive relation (14)) and the secondary load limit point exists before total collapse occurs. The evolution of diffuse plastic zones flattened the response curve within post-critical loading phase and increased the displacements.

The complexity of stress redistribution within the disk during propagation of the decohesive crack can be anticipated, when the patterns of diffuse plastic zones presented in Fig. 11a and b are compared. It is seen, that without decohesion the plastified elements create a band below applied external forces, when the limit capacity is approached. In the same region only few elements were plastified, when the decohesive cracks evolved, while the secondary plastic zone appears near the

symmetry axis AF. The later arises due to bending and tension of the deformed strip. This effect is more pronounced for lower values of L_v. In the case of $L_v = 0.2$ m the whole cross section AF was plastified before it was approached by the crack. As a result, the limit capacity below the load limit point was reached. From the numerical point of view the limit state was revealed by the numerically singular tangent stiffness matrix along the whole flat part of the response curve, see Fig. 12b. At the same time the selected matrix $\mathbf{C}_\rho$ was still well conditioned.

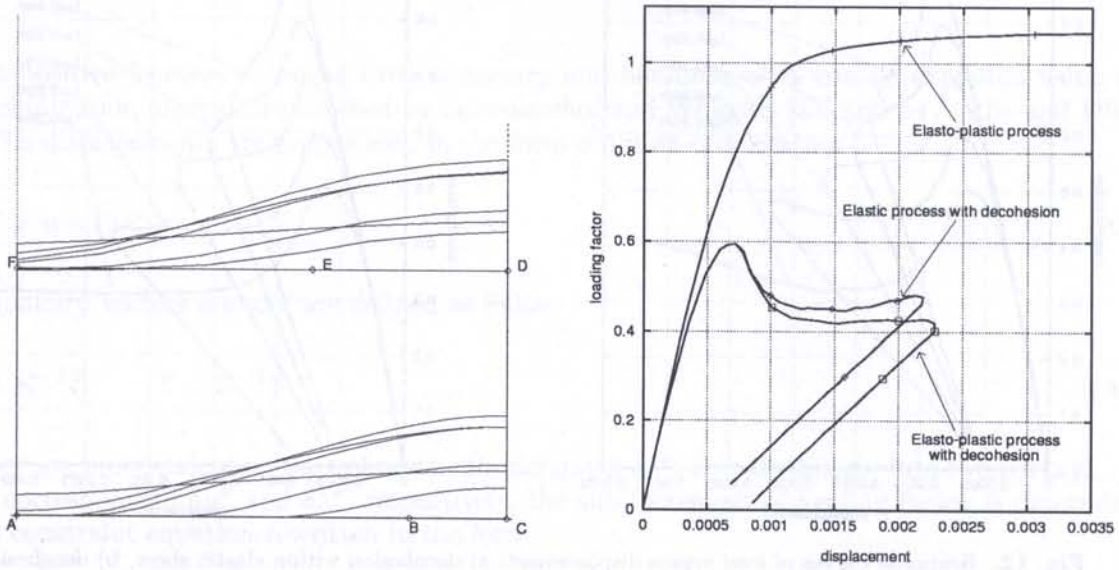

Fig. 10. a) Consecutive contour configurations, b) Response curves of load factor versus displacement; $L_v = 0.25$ m.

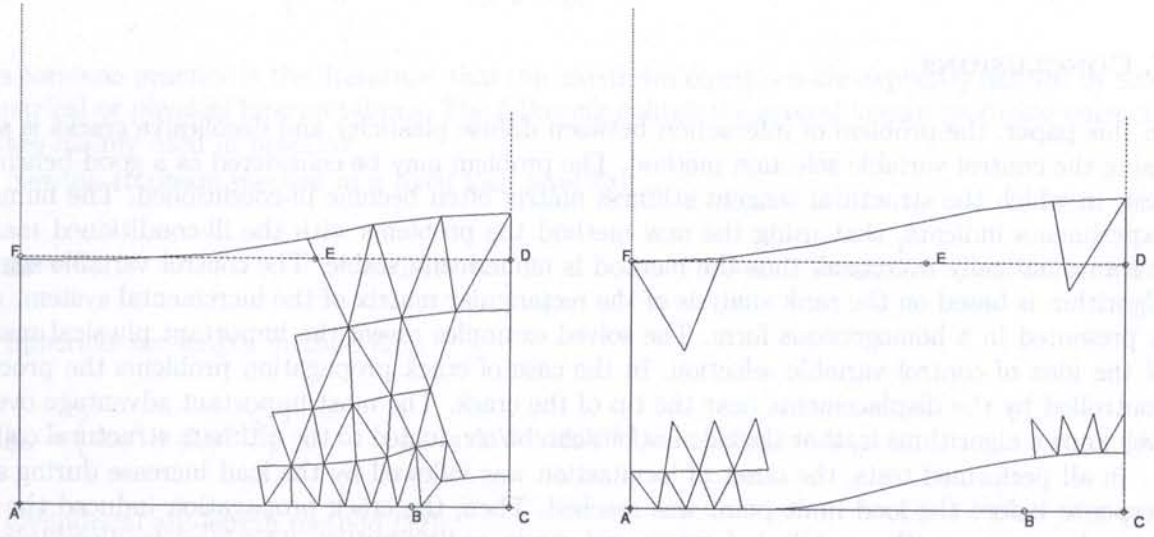

Fig. 11. Diffuse plastic zones within thin sheet made of: a) elastic-perfectly plastic material (decohesion neglected), b) elastic-perfectly plastic material; $L_v = 0.25$ m.

The last two figures, Fig. 12a and b, allow to compare the processes for different widths L_v. The underlined differences between two kind of processes, i.e. when diffusive plasticity is neglected and when it is taken into account, can be recognized for all presented curves. It is seen also, that in both cases the load limits are lower, while the displacements at the turning points increase for narrower strips. The higher displacements result from the stronger impact of diffuse plasticity. Note, that the radius of curvature of the graphs near the displacement turning points decreases with the

decreasing width L_v. In the extreme case for $L_v = 0.2$ m the ultimate zero load level could not be determined. In the case of elastic process, the algorithm could not overcome the sharp corner in the vicinity of turning point, while in the elasto-plastic process the limit capacity was reached as mentioned before.

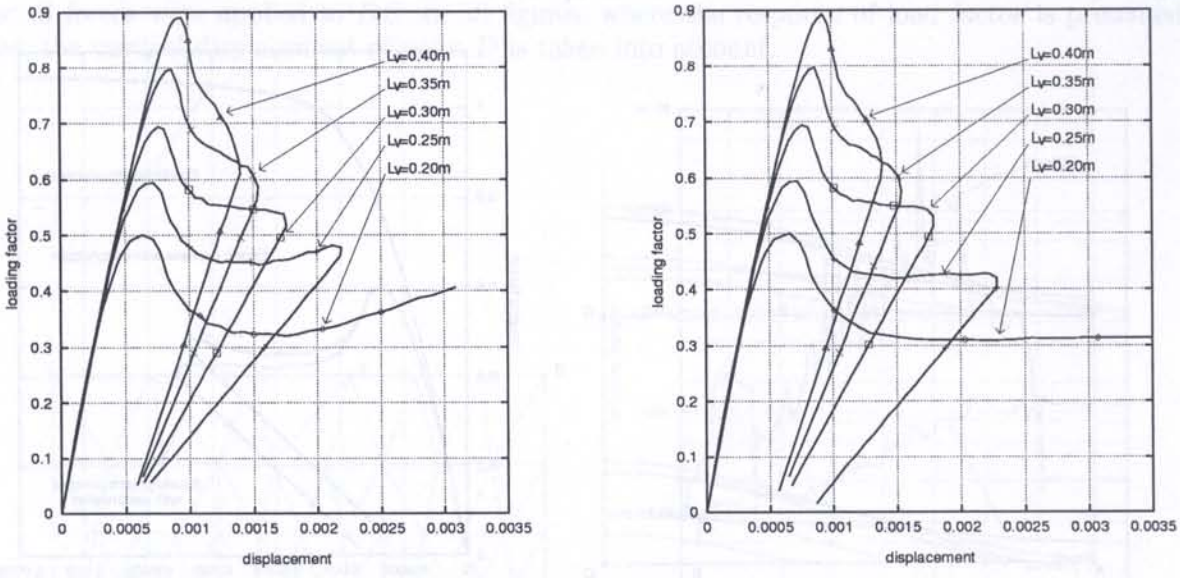

Fig. 12. Response curves of load versus displacement: a) decohesion within elastic sheet, b) decohesion within elastic-perfectly plastic sheet.

7. Conclusions

In this paper, the problem of interaction between diffuse plasticity and decohesive cracks is solved using the control variable selection method. The problem may be considered as a good benchmark test, in which the structural tangent stiffness matrix often become ill-conditioned. The numerical experiments indicate, that using the new method the problems with the ill-conditioned matrices are automatically overcome, thus the method is numerically stable. The control variable selection algorithm is based on the rank analysis of the rectangular matrix of the incremental system, which is presented in a homogeneous form. The solved examples reveal the important physical meaning of the idea of control variable selection. In the case of crack propagation problems the process is controlled by the displacements near the tip of the crack. The most important advantage over the well known algorithms is, that the calculations can be conducted to the ultimate structural collapse.

In all performed tests, the onset of localization was followed by the load increase during stable response before the load limit point was reached. Then, the crack propagation induced the post-critical response with complicated stress and strain redistribution. The local loading/unloading effects resulting from simultaneous development of the localized plastic flow and the diffuse plastic zones were observed. The interaction of two forms of plasticity is exhibited by the ultimate deformation of the sheet and the maximum load level achieved during the loading process. Both effects depend on geometrical and material parameters. The obtained results indicate, that even in a simple structure the primary load limit point may be followed by the subsequent load limit point during post-critical phase. Thus, the highest load level should be determined by the complete elasto-plastic analysis conducted to the ultimate failure. It can be expected, that in the case of complicated structures and for more realistic constitutive models the primary load limit level may not necessarily coincide with the structural capacity.

ACKNOWLEDGMENT

The research was supported by the State Committee for Scientific Research (KBN) in the framework of the Project N° 7 T07A 075 08.

APPENDIX – WELL KNOWN CONTINUATION SCHEMES

The positive features following from symmetry and bandness of $\mathbf{K}$ can be exploited using the block elimination algorithm proposed by Schweizerhof and Wriggers [25] and by Batoz and Dhatt [26]. The displacements are represented in the form of linear combination

$$\delta\mathbf{u}^{\nu} = \mathbf{e} + \mathbf{f}\delta\lambda^{\nu}. \tag{A.1}$$

The auxiliary vectors $\mathbf{e}$ and $\mathbf{f}$ are defined as follow

$$\mathbf{e} = \mathbf{K}^{-1}\mathcal{E}, \qquad \mathbf{f} = \mathbf{K}^{-1}\mathbf{F} \tag{A.2}$$

and they are independent on the unknown sub-increment $\delta\lambda^{\nu}$. By splitting $\mathbf{g}_N$ into two parts $\mathbf{g}_u$, g_λ, which correspond to $\delta\mathbf{u}^{\nu}$ and $\delta\lambda^{\nu}$, respectively, the sub-increment of loading factor is determined by the constraint equation rewritten in the form

$$(\mathbf{g}_u\mathbf{f} + g_\lambda)\delta\lambda^{\nu} + \mathbf{g}_u\mathbf{e} = \begin{cases} \Delta\eta_\omega & \text{for } \nu = 0, \\ 0 & \text{for } \nu > 0. \end{cases} \tag{A.3}$$

It is a common practice in the literature, that the constraint equations are explicitly defined by some geometrical or physical interpretations. The following defines the several known predictor-corrector schemes mainly used in practice:

- Newton-Raphson method at a fixed load level [20]:

$$\mathbf{g}_u = \mathbf{0}, \qquad g_\lambda = 1, \qquad \Delta\eta_\omega = \Delta\lambda_\omega. \tag{A.4}$$

- Spherical arc-length method [16]:

$$\mathbf{g}_u = \left(\Delta\mathbf{u}^{\nu} + \Delta\mathbf{u}^{\nu+1}\right)^T, \qquad g_\lambda = \Delta\lambda^{\nu} + \Delta\lambda^{\nu+1}, \qquad \Delta\eta_\omega = \Delta s_\omega. \tag{A.5}$$

- Cylindrical arc-length method [22]:

$$\mathbf{g}_u = \left(\Delta\mathbf{u}^{\nu} + \Delta\mathbf{u}^{\nu+1}\right)^T, \qquad g_\lambda = 0, \qquad \Delta\eta_\omega = \Delta s_\omega. \tag{A.6}$$

In the above, Δs_ω is the specified arc-length measured along the solution path in the displacement-loading factor space in the case of spherical arc-length method and along the respective projection of the solution path in the space of displacements in the case of cylindrical arc-length method. It is known, that the explicit formulations may result with the incompatible augmented incremental systems.

REFERENCES

[1] A. Needleman. A continuum model for void nucleation by inclusion debonding, *J. Applied Mechanics*, **54**: 525–531, 1987.

[2] V. Tvergaard. Necking in tensile bars with rectangular cross-section. *Computer Methods in Applied Mechanics and Engineering*, **103**: 273–290, 1993.

[3] M. Życzkowski, Tran-le Binh. Interaction curves corresponding to the decohesive carrying capacity of a cylindrical shell under combined loading, *Int. J. Plasticity*, (1997), to appear.

[4] M. Życzkowski, K. Szuwalski. On the termination of the process of finite plastic deformations, *J. Méc. Theor. Appl.*, **1**: 175–186, 1982.

[5] H. Schreyer, Shijian Zhou. A unified approach for predicting material failure and decohesion, *AMD-Vol. 200/ MD-Vol. 57, Plastic and Fracture Instabilities in Materials*, ASME 1995.

[6] R. Hill. On discontinuity plastic states, with special reference to localized necking in thin sheets, *J. Mech. Phys. Solids*, **1**: 19–30, 1952.

[7] Z. Mróz, M. Kowalczyk. Elasto-plastic post-critical analysis of disks under tension, *Arch. Mech.*, **41**: 461–480, 1989.

[8] S. E. Clift, P. Hartley, C. E. N. Sturgess, G. W. Rowe. Fracture prediction in plastic deformation process, *Int. J. Mech. Sci.*, **32**: 1–17, 1990.

[9] J. Desrue. Localization de la déformation dans les matériaux granulaires, *Thèse de doctorat USMG*, Grenoble, 1984.

[10] D. Bigoni, T. Hueckel. Loss of uniqueness and shear band in associative and non-associative plasticity, 2^{nd} International Workshop on *Numerical Methods for Localization and Bifurcation of Granular Bodies*, 31–40, 1989.

[11] K. Runesson, N. S. Ottosen, D. Perić. Discontinuous bifurcation of elastic-plastic solutions at plane stress and plane strain, *Int. J. Plasticity*, 99–121, 1991.

[12] K. Szuwalski. Decohesive carrying capacity of annular axially-symmetrical disc with rigid inclusion (in Polish), *Mech. Teor. Stos.*, **17**: 589–602, 1979.

[13] R. Seydel. *From Equilibrium to Chaos. Practical Bifurcation and Stability Analysis*, Elsevier, 1988.

[14] M. A. Crisfield. *Nonlinear finite element analysis of solids and structures, Volume 1: Essentials*, John Wiley & Sons, 1991.

[15] E. Hinton (ed.). Introduction to Nonlinear Finite Element Analysis, NAFEMS, Bell & Bain Ltd, 1992.

[16] E. Riks. The application of Newton's method to the problem of elastic stability, *J. Appl. Mech.*, **39**: 1060–1065, 1972.

[17] J. Lubliner. *Plasticity Theory*, Macmillan Publishing Company, New York, 1990.

[18] M. Kowalczyk. Rank analysis of rectangular matrix as an element of continuation method, *Engineering Computations*, **10**: 61–80, 1993.

[19] M. Kowalczyk. Nonlinear analysis based on homogeneous incremental systems, *Int. J. Comp. Meth. Appl. Mech. Engng*, **156**: 277–297, 1998.

[20] D. W. Murray, E. L. Wilson. Finite-element large deflection analysis of plates, *Proc. ASCE, J. Engng. Mech. Div.*, **95**(EM1): 143–165, 1969.

[21] H. Chen, G. E. Blandford. Work-incremental-control method for non-linear analysis, *Int. J. Numer. Meth. Engng.*, **36**: 909–930, 1993.

[22] M. A. Crisfield. An arc-length method including line searches and accelerations, *Int. J. Numer. Meth. Engng.*, **19**: 1269–1289, 1983.

[23] W. F. Lam, C. T. Morley. Arc-length method for passing limit points in structural calculation, *J. Structural Engineering*, **118**: 169–185, 1992.

[24] S. R. Kuo, Y. B. Yang. Tracing postbuckling paths of structures containing multi-loops, *Int. J. Numer. Meth. Engng.*, **38**: 4053–4075, 1995.

[25] K. H. Schweizerhof, P. Wriggers. Consistent linearization for path following methods in nonlinear FE analysis, *Comput. Meth. Appl. Mech. Engng.*, **59**: 261–279, 1986.

[26] J.-L. Batoz, G. Dhatt. Incremental displacement algorithms for nonlinear problems, *Int. J. Num. Methods Engng.*, **14**: 1262–1267, 1979.

[27] G. E. Forsythe, M. A. Malcolm, C. B. Moler. *Computer Metods for Mathematical Computations*, Prentice-Hall, 1977.